Published in final edited form as:
J Mol Biol. 2008 November 21; 383(4): 854–870. doi:10.1016/j.jmb.2008.08.059.

X-ray crystal structure of a TRPM assembly domain reveals an antiparallel four-stranded coiled-coil

Yuichiro Fujiwara and **Daniel L. Minor Jr.***
Cardiovascular Research Institute, Departments of Biochemistry and Biophysics & Cellular and Molecular Pharmacology, California Institute for Quantitative Biosciences, University of California San Francisco, San Francisco, California 94158-2330, USA

Abstract

Transient receptor potential (TRP) channels comprise a large family of tetrameric cation-selective ion channels that respond to diverse forms of sensory input. Previous studies have shown that members of the TRPM subclass possess a self-assembling tetrameric C-terminal cytoplasmic coiled-coil domain that underlies channel assembly and trafficking. Here, we present the high-resolution crystal structure of the coiled-coil domain of the channel enzyme TRPM7. The crystal structure, together with biochemical experiments, reveals an unexpected four-stranded antiparallel coiled-coil architecture that bears unique features relative to other antiparallel coiled-coils. Structural analysis indicates that a limited set of interactions encode assembly specificity determinants and uncovers a previously unnoticed segregation of TRPM assembly domains into two families that correspond with the phylogenetic divisions seen for the complete subunits. Together, the data provide a framework for understanding the mechanism of the TRPM channel assembly and highlight the diversity of forms found in the coiled-coil fold.

Keywords

TRP channel; X-ray crystallography; coiled-coil; assembly domain

INTRODUCTION

Transient receptor potential (TRP) channels form a diverse family of nonselective cation channels that contribute to a range of sensory processes including thermosensation, phototransduction, chemosensation, and nociception[1; 2; 3]. These channels are members of the superfamily that includes voltage-gated channels for calcium, potassium, and sodium, as well as cyclic nucleotide-gated channels[4; 5]. As with other members of the superfamily, TRP channels are thought to be composed of four pore-forming subunits[6; 7], an idea supported by the recent identification of TRPM subfamily tetrameric cytoplasmic assembly domains[8] and low-resolution cryo-EM studies of TRPV1[9].

*Correspondence: daniel.minor@ucsf.edu.

Accession Code:
Coordinates and structure factors have been deposited with the PDB structure code 3E7K.

Members of the TRPM subfamily[10; 11] include channels that respond to cold, TRPM8[12], are involved in taste, TRPM5 [13; 14], channel-kinases that are important for divalent cation uptake, TRPM6 and TRPM7 [15; 16; 17; 18; 19; 20], and channels that act as redox sensors, TRPM2[21; 22]. Concomitant with their diverse functions, TRPM channels have diverse C-terminal domains but share a C-terminal cytoplasmic tetrameric coiled-coil that self-assembles and directs channel assembly[8; 23; 24]. Coiled-coils are a widespread protein-protein interaction structural motif and are found in disparate protein classes that include fibrous proteins, motor proteins, transcription factors, and membrane fusion proteins[25; 26]. Beyond the varied biological roles, the regularity of the coiled-coiled structure has made coiled-coils a favorite model system for understanding protein sequence-structure relationships, deciphering interaction specificity determinants, and protein engineering efforts[26; 27; 28]. The involvement of cytoplasmic coiled-coil domains as key elements of ion channel assembly is an emerging theme with a examples found in diverse members of the voltage-gated ion channel superfamily such as: TRPM channels[8; 23; 24], Kv7 channels[29; 30; 31], Eag channels[31; 32], CNG channels[33; 34], polycystins[35; 36], and in the voltage-sensor only proton channel Hv1[37].

Many ion channels are composed of multiple pore-forming subunits and recurrently, incorporation of different subunit types has profound effects on the functional properties of the resulting channel. Understanding how elements in the individual subunits guide channel assembly and specify subunit assembly preferences is an incompletely understood problem. To date, two cases have been characterized structurally, T1 domain of Kv1-Kv4 channels[38; 39; 40; 41] and coiled-coil domains from Kv7 (KCNQ) channels[29; 30]. The presence of cytoplasmic coiled-coil domains in diverse voltage-gated ion channel superfamily members suggests that this type of domain has a predominant role in directing pore-forming subunit assembly.

Here, we report the structure of the coiled-coil assembly domain from the channel-kinase TRPM7[15; 16; 17], a divalent cation-permeable channel that is expressed in a wide variety of tissues including the brain, heart, kidney, and hematopoietic organs[17; 42; 43]. TRPM7 channels conduct calcium and magnesium ion influx into cells, are tonically inhibited by intracellular Mg^{2+} ions and Mg-complexed nucleotides, and are modulated by a variety of factors that include acidic pH, phosphatidylionsitol bisphosphate (PIP_2). and phosphlipase C pathways[42]. TRPM7 activity supports multiple physiological functions that include Mg^{2+} homeostasis[44; 45], cell viability and growth[15; 45], anoxic neuronal cell death[46], intestinal pacemaking[47], and skeletogenesis[48]. In addition to its plasma membrane roles, TRPM7 has been found in chlolinergic synaptic vesicles where its activity may regulate the amount of mobile transmitter contained therein[49]. TRPM7 dysfunction is linked to familial Alzheimer's disease (FAD)[50; 51] and may have a role in hypertension[52]. Additionally, TRPM7 forms functional heteromultimers with TRPM6[18; 19; 20], a subunit in which mutations lead to the Mg^{2+} absorption/reabsorption disorder, Hypomagnesemia with Secondary Hypocalcemia (HSH)[18; 53; 54]. Thus, understanding how TRPM7 assembles alone and as heteromultimers with TRPM6 is important for both understanding the basic mechanisms of TRPM channel assembly and TRPM channelopathies.

We find that the TRPM7 assembly domain, TRPM7cc, is an antiparallel coiled-coil having an unprecedented coiled-coil architecture that is largely symmetric in the middle but that diverts at the ends into a diamond-shaped packing arrangement coincident with an alternating ‘knobs-against-knobs’ packing arrangement of the core ‘a’ and ‘d’ positions. The D2 symmetry in the TRPM7cc antiparallel arrangement does not match the expected rotational four-fold symmetry of the pore but is in accord with the two-fold symmetry found in the kinase domain that lies just C-terminal to the coiled-coil [55]. Structure and assembly determinants of antiparallel coiled-coils are less well understood than their parallel counterparts in part due to a limited

number of examples[26; 28]. The TRPM7cc structure highlights the remarkable structural diversity found in coiled-coils and should serve as a framework to begin to understand the structural basis for TRPM channel assembly specificity.

RESULTS

Crystal Structure of the TRPM7 Assembly Domain

TRPM C-terminal cytoplasmic domains have varied lengths and domain compositions (Figure 1A). In the midst of this architectural diversity resides a coiled-coil domain that is well conserved in terms of its position in the C-terminal cytoplasmic domain, ~100 residues C-terminal to the last transmembrane segment of the pore-forming domain, and clear heptad repeat pattern, denoted $(abcdefg)_n$ [8] (Figure 1A, B). Even though coiled-coils can be readily identified from sequence analysis by the presence of the distinctive heptad repeat, $(abcdefg)_n$ in which 'a' and 'd' positions are hydrophobic amino acids[25; 56], accurate prediction of coiled-coil three-dimensional structure and assembly preferences from sequence remains elusive[25; 27]. In order to begin to understand the architecture that underlies the TRPM assembly domain, we expressed, purified, and crystallized a rat TRPM7 coiled-coil domain construct, TRPM7cc (residues 1230–1282).

Vapor diffusion crystallization gave two TRPM7cc crystal forms, monoclinic C121 and orthorhombic C222, that diffracted synchrotron X-rays to 2.00 and 2.40 Å, respectively. Structure determination by molecular replacement using several types of parallel four-stranded coiled-coils failed. Therefore, we grew crystals of TRPM7cc in which selenomethionine was biosynthetically incorporated. Selenomethionine substituted TRMP7cc crystals grew in the C222 form and diffracted X-rays to 2.8Å resolution (Table I). Structure solution using experimentally determined phases from a three wavelength MAD experiment gave readily interpretable electron density maps in which the α-helical backbone, side chains, and selenomethionine positions were visible (Figure 1C). The maps further revealed that the single selenium atoms from in each chain were clustered into pairs at both ends of an antiparallel tetrameric coiled-coil (Supplemental Figure 1) and provided a clear explanation for why molecular replacement using parallel four-stranded coiled-coils failed. An initial structural model from the C222 crystal form experimental electron density was built using Arp/Warp[57] and refined for several cycles. The resulting model was used to solve the structure of the C121 crystal form, which diffracted X-rays to higher resolution than the C222 form, by molecular replacement using Phaser[58] (Figure 1D). The C121 asymmetric unit contains two tetramers. We were able to build all of the backbone atoms for all eight polypeptides, excepting a few terminal residues and a few sidechains (Supplementary Figure 2), and refine the resulting model to an acceptable level (R/R_{free} = 18.8 / 24.8%) (Table I).

Core packing analysis and comparison with other antiparallel tetramers

The overall structure of TRPM7cc is that of a tightly twisted, symmetrical, antiparallel left-handed four-stranded coiled-coil that is 25 Å wide and 77 Å long (Figure 1E, 2A). The tetramer interface shows a classical antiparallel coiled-coil pattern in which the 'a' and 'd' positions comprise layers along the superhelical core composed of pairs of diagonally opposed 'a' position residues and 'd' position residues (Figure 2A, B).

Three different anti-parallel four-stranded coiled-coils core-packing architectures have been described, the 'a-d' core, 'e-a-d' core, and 'a-d-g' core (Figure 2C), each of which has a distinct buried surface area pattern among the heptad positions[59]. Position specific analysis of buried surface area relative to an isolated α-helical strand shows that the TRPM7cc quaternary structure completely buries the 'a' and 'd' positions as well as a substantial amount of the surface area of the 'e' and 'g' positions (Table II). In contrast, 'b', 'c', and 'f' positions along

the exterior surface of the helical bundle remain highly exposed. These features classify TRPM7cc as an 'a-d' core coiled-coil. Relative to the three other known 'a-d' core four-stranded anti-parallel structures, WSPLP[60], GCN4-E20C[61], and Rop[62], the amount of burial at the TRPM7cc positions that flank the core ('e' vs. 'g' and 'b' vs. 'c'), is much more uniform (Table II).

Each TRPM7cc a-d layer comprises two 'a' and two 'd' position residues. Notably, there are substantial differences in the way the components of the layers pack as one progresses from the center layers to the layers near the strand termini. In the middle region, Layers 1 and 2, the 'a' and 'd' position side chains interact in the classical 'knobs-into-holes packing'[63] (Figure 2B). In this portion of the structure, the individual strands of the coil form a square-like symmetrical shape. However, near the coiled-coil ends, Layers 5→7, the core packing geometry changes to the "knob-against-knob packing" in which the 'a' or 'd' positions directly face each other[25; 59; 64] (Figure 2B). Furthermore, the sidechain positions that oppose each other through the "knob-against-knob" interactions alternate from layer to layer (e. g. Layer 5 'd' positions interact whereas Layer 6 'a' positions interact). Other 'a-d' core antiparallel tetramers show only one type of the "knob-against-knob packing" involving either the side chains at 'a', GCN4-E20C[61] and WSPLP[60], or 'd', Rop[62], positions. Thus, the TRPM7cc layer-by-layer alternation in packing is unique among antiparallel coiled-coils (Table II).

Along with the packing changes in the terminal layers, the arrangement of the individual strands differ from that found in the center of the helical bundle. Rather than the symmetrical square arrangement seen in Layers 1 and 2, the terminal parts of the individual strands of the coil are arranged in a diamond shape in which the C-terminal strands are more peripheral whereas the N-terminal strands are in the center (Figures 2B and 2D). Each of the three final layers (5→7) includes two buried, polar residues. In each case, the buried, polar residue is involved in hydrogen bonding interactions. S1271 (Layer 5) makes an interaction with a buried water molecule that is bridged to either the sidechain carbonyl of Gln1268 from the same strand or the backbone carbonyl of V1236 from the adjacent strand. Each interaction is seen in two of eight possible incidences. In contrast, Layer 6 and Layer 7 hydrogen bond interactions are present in all eight possible occurrences in the asymmetric unit. Thr1264 in Layer 6 makes a hydrogen bond to the carbonyl oxygen of L1270 from its own helix. Thr1232 (Layer 7) is part of a hydrogen bond network (see below). It seems likely that the difference in the strand arrangement between the center and ends of the coil is linked to the incorporation of the hydrophilic residues in the core.

Comparison of the TRPM7cc superhelical parameters with previously determined antiparallel homo-tetramer coiled-coil structures shows that TRPM7cc is more tightly packed and more twisted than other antiparallel coiled-coils (Table II). These factors, together with the unique packing and strand divergence indicate that the TRPM7cc structure is unique among the 'a-d' core antiparallel tetrameric coiled-coils and underscore the structural diversity inherent in the coiled-coil fold[27].

Electrostatic interactions

The TRPM7cc surface is composed predominantly of polar residues. A number of these are used in three distinct sets of side chain hydrogen bond networks that form across helix interfaces within the coiled-coil bundle (Figure 3). The central component of 'Network 1' is Arg1235, a 'g' position. This residue interacts with the sidechain hydroxyl of Thr1277 a 'g' position from the neighboring helix and a buried water molecule that makes bridging hydrogen bonds to the Thr1274 carbonyl oxygen in the adjacent helix and the d' position Thr1232 sidechain hydroxyl from the Arg1235 bearing helix. This network is observed in all eight possible copies in the asymmetric unit. 'Network 2' involves three side chains; Asn1251 and Lys1254, 'b' and 'e' positions from one strand, interact with Asp1261 an 'e' position, from the adjacent strand and

is arranged in two configurations. Of the eight possible Network 2 occurrences, the tripartite arrangement occurs five times. The remaining three lack one substituent but retain cross-strand interactions that involve either the Asn1251-Asp1261 'b-e' or Lys1254-Asp1261 'e-e' pairs. 'Network 3' involves three sidechains: Glu1245 and Arg1249, 'c' and 'g' positions from same strand and Gln1263 a 'g' position from the adjacent strand. 'Network 3' displays two configurations in which the participating sidechains interact. In one, 'Network 3a' (Figure 3), two substituents from the same chain interact (Glu1245 and Arg1249) and Arg1249 makes a bidentate hydrogen bond to Gln126 from the adjacent helix. The Network 3a arrangement occurs in six instances; however, two of these lack the intra-subunit Glu1245-Arg1249 hydrogen bond. In the other configuration, 'Network 3b' (Figure 3), which is observed twice, Gln1263 is pinned between Arg1249 and Glu1245 from the adjacent strand. In addition to these intersubunit interactions, we observed an intrasubunit salt bridge between 'b' and 'f' positions Arg1230 and Glu1234 in the first turn of the helix in six of the eight copies in the asymmetric unit.

Structure-based comparison of TRPM coiled-coils uncovers two subfamilies

Structure-based comparison of the coiled-coil regions from the TRPM subtypes (Figure 4A) reveals that even though all possess a coiled-coil domain, the TRPM coiled-coil domains segregate into two groups: those having TRPM7 features (TRPM1, TRPM3, and TRPM6, denoted the 'TRPM7 group') and those that not like TRPM7 (TRPM2, TRPM4, TRPM5, and TRPM8, denoted the 'TRPM8 group'). In light of the TRPM7cc structure, the most obvious difference between the groups is that the TRPM8 group has coiled-coil domains that are shorter than the TRPM7 group by 1-1.5 heptad repeats (Figure 1A).

Within the TRPM7 group, TRPM6 is most similar to TRPM7. Five of the seven 'a-d' layers (layers 1, 2, 5, 6, and 7) are identical and the remaining two (layers 3 and 4) have conservative, hydrophobic changes. Amino acids that form the three interhelix electrostatic interaction networks are also well conserved (Figure 4A). The core and interhelix hydrogen bond compatibilities are consistent with observation that TRPM7 and TRPM6 subunits interact to form heteromeric channels[18; 19; 20]. With the exception of layer 2, TRPM1 and TRPM3 coiled-coil domains have 'a' and 'd' position sidechains compatible with the TRMP7cc core. TRPM1 and TRPM3 retain residues that could form the Network 2 interaction but lack appropriate sidechain chemistry for making Network 1 and Network 3. Together, such differences may help to specify assembly preferences among the closely related TRPM7 group coiled-coil domains.

Consideration of the TRPM8 core residues in the context of the TRMP7cc antiparallel framework shows a remarkably poor conservation (Figure 1B and Figure 4A). The incompatibilities extend to the electrostatic contacts. Together with the apparent differences in coiled-coil lengths and prior biochemical results that establish the tetrameric self-assembly properties of TRPM8 subgroup members[8], it seems likely that the TRPM8 subgroup has a coiled-coil quaternary structure different from the TRPM7 group. Interestingly, the class differences we find between the TRPM7 and TRPM8 groups from the structure-based comparison of the assembly domains are reflected in phylogenetic analyses of full-length TRPMs[1; 10; 11] (Figure 4B). Additionally, the close conservation of the TRPM7-TRPM6 and TRPM1-TRPM3 coiled-coil pairs is reflected by the full channel comparison. As the coiled-coils (~50 residues) are only a fraction of the total channel subunit sequence (~1,000 residues), correspondence between the overall TRPM family tree and the relationships of the coiled-coils suggests that the relative divergence of the coiled-coil sequences has paralleled other changes within the channel subunit. This observation reinforces the idea that interactions between the coiled-coil strands are likely to be important TRPM assembly specificity determinants.

TRPM7cc is an antiparallel tetramer in solution

There are a number of cases in which crystal structures of engineered coiled-coils did not represent the only or even the major species that present in solution[60; 61]. Therefore, we used a number of biochemical and biophysical measures to probe the structure and assembly properties of TRPM7cc in aqueous solution. Measurement of the TRPM7cc circular dichroism (CD) spectrum reveals minima at 208 and 222 nm that are characteristic of a protein with high helix content (Figure 5A). Estimation of helix content[65] indicates that the peptide is 92.2% helical. This value is in good agreement with the structure where each helix contains fifty residues (Arg1230–Lys1279) that comprise 87.7% of the fifty-seven residue peptide. Further, the temperature dependence of the CD signal shows a cooperative loss of structure, consistent with a well-folded complex having an extensive hydrophobic core as seen in the crystal structure (Figure 5B).

Size exclusion chromatography of TRPM7cc showed a single peak with an apparent molecular mass that is consistent with a tetramer (Figure 5C) in agreement with the crystallographically observed stoichiometry. Size exclusion relies on the hydrodynamic radius. Because comparison of an elongated protein assembly, such that formed by TRPM7cc, to the globular protein size standards used in the size exclusion experiments has some uncertainty, we used sedimentation equilibrium experiments, a method that is shape-insensitive[66], to attain a precise measurement of the assembly state of TRPM7cc in solution. Over a range of concentrations, the TRPM7cc equilibrium sedimentation data were well-fit by a single species model having the molecular mass of a tetramer (Figure 5D, Table III). These data establish the tetrameric nature of TRPM7cc in solution.

To probe whether TRPM7cc tetramers assembled in the antiparallel orientation in solution, we used a disulfide exchange assay that reports on the relative helix orientation within the bundle (Figure 6A)[61; 67; 68; 69; 70]. We expressed and purified TRPM7cc variants in which a single cysteine residue was added to the N-terminus (N-TRPM7cc) or C-terminus (C-TRPM7cc) via a Gly-Gly-Ser linker. These peptides were used in subunit exchange experiments in which complexes containing either oxidized N-TRPM7cc or C-TRPM7cc homodimers were mixed, reduced, allowed to exchange partners, and reoxidized. Figure 6A depicts the equilibria and expected species for the antiparallel and parallel cases following the exchange of reduced subunits and disulfide bond reformation. The presence of antiparallel tetramers results in the creation of a unique heterodimeric disulfide linked species N-TRPM7cc/C-TRPM7cc that is absent from the parallel arrangement. HPLC and mass spectrometry analysis shows that a new peak that corresponds to disulfide liked N-TRPM7cc/C-TRPM7cc heterodimer, N-C, appears following the initial mixing of N-TRPM7cc and C-TRPM7cc homotetramers composed of only N-N and C-C dimers (Figure 6B). The N-C antiparallel peak becomes the dominant disulfide-bonded species as the system reaches equilibrium and provides an unambiguous signature of the presence of antiparallel quaternary structure in solution. Taken together, these data establish that the TRPM7 assembly domain is a helical antiparallel tetramer in solution that mirrors the crystal structure and the expected stoichiometry of tetrameric TRPM channels.

Discussion

The presence of cytoplasmic domains that direct channel assembly appears to be a feature of many voltage-gated ion channel superfamily members. Because the assembly of different combinations of pore-forming subunits can have profound effects on channel functional properties, it is critical for members of this channel class to encode assembly determinants that direct association with the appropriate partners[4; 19; 71; 72; 73]. Despite the fundamental nature of this problem, the mechanisms that drive channel assembly and assembly specificity remain imperfectly understood. To date, two different types of assembly domains have been characterized structurally, the ‘T1 domain’ a tetramerization and assembly specificity domain

found in Kv1-Kv4 channels[38; 39; 40; 41] and the Kv7 (KCNQ) coiled-coil assembly specificity domain [29; 30]. Coiled-coils have been identified in a number of other voltage-gated superfamily members that include TRPM channels[8; 23; 24], Eag channels[31; 32], CNG channels[33; 34], polycystins[35; 36], and in the voltage-sensor only proton channel Hv1[37] and suggest that the coiled-coil motif is the predominant means for mediating pore-forming subunit assembly in this superfamily.

TRPM7cc is a four-stranded antiparallel coiled-coil that is held together by extensive core packing and interstrand polar interactions. Three types of core packing have been reported for homotetrameric antiparallel coiled-coils, ‘a-d’, ‘e-a-d’ and ‘a-d-g’ (Figure 3B). Two classes, ‘e-a-d’ and ‘a-d-g’ cores, have been proposed to arise when either the ‘e’ positions[74], or ‘g’ positions[59] contain largely nonpolar residues, respectively. TRPM7cc has the ‘a-d’ packing and bears ‘e’ and ‘g’ amino acids that are mostly polar and incompatible with the ‘e-a-d’ and ‘a-d-g’ modes. Comparison of ‘a-d’ four-strand antiparallel bundles further shows the architectural diversity that can arise even when the basic core of the assembly is similar. TRPM7cc structure buries the surface area of the ‘e’ and ‘g’ positions in a more symmetrical way than other ‘a-d’ core coiled-coils (Table II, Supplementary Figure 3).

One of the striking features of TRPM7cc profile of the TRPM7 structure is the gradual change in the strand arrangement from square-shaped symmetry in the middle layers to a diamond-shape in the end layers (Figure 2D). This change occurs in conjunction with changes in core packing from ‘knobs-into-holes’ to ‘knobs-against-knobs’ and an unusual layer-to-layer alternation regarding which residues participate in the ‘knobs-against-knobs’ packing. One possible source for the change is that the volumes of the side chains in the middle layers are similar whereas there are larger mismatches (e.g. Layer 5 Met/Ser) at the ends. Additionally, layers 5–7 contain polar core residues that are involved in a variety of interactions with positions outside of the core. Such features may also contribute to the change in helix packing arrangement.

Even though coiled-coils are the most common and best understood protein-protein interaction domain[25; 26] and there are a number of robust algorithms for identifying coiled-coil sequences, the ability to predict the association state and assembly orientation of a given coiled-coil sequence remains elusive[27]. The unique structural features of TRPM7cc highlight the diversity of assembly architectures that can be encoded in a coiled-coil sequence.

Insights into subunit assembly preferences

TRP channels form the largest and most diverse subfamily within the voltage-gated ion channel superfamily[1]. In accord with other family members, TRP channels are thought function as homotetramers or heterotetramers of pore-forming subunits. Analysis of TRPM coiled-coil assembly domains through the lens of the TRPM7cc structure reveals that TRPM coiled coil assembly domains cluster into two families, the TRPM7 group (TRPM1, TRPM3, TRPM6, and TRPM7) and the TRPM8 group (TRPM2, TRPM4, TRPM5, and TRPM8). Gross differences in the coiled-coil lengths and incompatibilities in hydrophobic core compositions suggest that the TRPM7 and the TRPM8 groups are have different quaternary structures and that there is unlikely to be co-assembly between group members. Because of the extensive differences, it is unclear from the comparison whether the TRPM8 group forms parallel or anti-parallel tetramers.

In contrast, the presence of extensively conserved sidechain chemistries among ‘a-d’ core and interstrand polar interaction network residues indicates good structural compatibility between TRPM7 and TRPM6 coiled-coils. This assembly domain similarity matches the ability of these two channel subunits to form functional heteromultimers[18; 19; 20]. The other two members of the TRPM7 group, TRPM1 and TRPM3, appear more similar to each other than to TRPM7.

Although the TRPM1 and TRPM3 coiled-coil 'a-d' core residues have a good deal of similarity to TRPM7cc, the inclusion of bulky and polar amino acids, Met and Glu, Layers 1 and 2 (Figure 4A) might be incompatible with the very regular square arrangement of the strands in the part of the coil. Further TRPM1 and TRPM3 lack ability to form Network 1 and Network 3 interactions (Figure 4B). The similarities between TRPM1 and TRPM3 assembly domains raise the possibility that these subunits form heteromeric channels. The most striking observation from the structure-based comparison of the TRPM assembly domains is that the relationships found in the assembly domains reflect the phylogenetic relationships among the full-length subunits (Figure 4). This observation lends support to the idea that the assembly domains carry information for directing assembly specificity.

Relationship of the TRPM7cc antiparallel assembly to other TRPM domains and ion channel assembly domains

Structural studies have elucidated three different assembly domain architectures employed to specify assembly and assembly preferences of individual pore forming subunits within the voltage-gated channel superfamily: tetramers of the Kv1-Kv4 T1 domain[38; 41; 75], Kv7 channel parallel tetrameric coiled-coils[29; 30], and TRPM7 antiparallel coiled-coils. Because Kv7 coiled-coil assembly domains are parallel tetramers having approximate C4-symmetry that matches the expected symmetry of the voltage-gated channel superfamily pore forming domains, it was unexpected to find that the TRPM coiled-coil assembly domain TRPM7cc is an antiparallel coiled-coil having D2-symmetry (Figure 7). Although at first glance the antiparallel coiled-coil assembly domain might seem incompatible with the pore architecture, TRPM7cc resides ~100 residues distal to the end of the last transmembrane segment, S6. This intervening linker is sufficiently long to ease any requirement for an exact symmetry match between the assembly domain and the pore-forming subunit. It is notable that the arrangement of the TRPM7cc C-terminal ends is compatible with the symmetry of the immediately downstream kinase domains that forms dimers[55] (Figure 7A). Thus, the antiparallel coiled-coil assembly would be a suitable linker between the tetrameric transmembrane region and the dimer cytoplasmic enzyme domain. Given the similarities between TRPM7, TRPM6, TPRM1, and TRPM3 coiled-coils, it seems likely that similar antiparallel arrangements exist for this subclass.

Both Kv1-Kv4 T1 domains[76; 77; 78] and Kv7 coiled-coil assembly domains[79; 80; 81] form platforms for the recruitment of regulatory molecules to the channel. The importance of such protein complexes is underscored by the observation that some disease mutations reside on the exterior of the Kv7 coiled-coil assembly and rather than act by blocking channel assembly, interfere with regulatory protein binding[29; 30]. It seems likely that TRPM coiled-coil assembly domains will perform a similar role in the recruitment of TRPM modulatory proteins and may harbor channelopathy mutations. The structure we present here of TRPM7cc should serve as a useful starting point for focusing questions about TRPM channel assembly, assembly specificity, interactions to cytosolic regulatory factors, and in understanding the roles of TPRM channels in human diseases.

Materials and Methods

Protein Cloning, Expression, and Purification

DNA corresponding to the of TRPM7 coiled-coil domain (residues 1230–1282) was amplified by PCR and ligated into the NarI/HindIII sites of a pET27 (Novagen) derived vector (pSV272) denoted 'HMT' [82] that contains, in sequence, a hexahistidine tag, maltose binding protein, and a cleavage site for the Tobacco Etch Mosaic Virus (TEV) protease. As a consequence of the cloning sites the constructs retain an extra N-terminal sequence 'GAGS' following TEV cleavage of the purified protein. Point mutations were made using oligonucleotide extension

(Pfu Turbo Polymerase, Strategene), digested with DpnI (New England Biolabs), and transformed into DH5α cells, and verified by DNA sequencing.

HMT fusions were expressed in *Escherichia coli* [BL21(DE3)pLysS] grown in 2YT at 37°C and induced at OD_{600nm} = 0.4–0.8 with 0.4 mM IPTG for 4 hrs. SeMet-TRPM7 protein was expressed in PASM-5052 auto_induction medium (50 mM Na_2HPO_4, 50 mM KH_2PO_4, 25 mM $(NH_4)_2SO_4$, 2 mM $MgSO_4$, 0.5 % glycerol (v/v), 0.05 % glucose (w/w), 0.2 % lactose (w/w), 0.2x trace metal mix, 200 mg/ml of each of seventeen amino acids except cysteine and tyrosine, 10 mg/ml methionine, 125 mg/ml SeMet, and 100 nM vitamin B12)[83] for 24 hours. Cells were harvested by centrifugation, 15' 5000 × g at 4°C, and cell pellets were frozen at −20°C. Thawed cell pellets were lysed by sonication in lysis buffer (20 mM Tris pH 8.0, 250 mM KCl, 10% sucrose, 1 mM EDTA, 1 mM PMSF). Insoluble material was precipitated by centrifugation, 20' 12,000 × g at 4°C. The resulting soluble fraction, which contained the HMT fusion protein, was applied to a 45 ml Poros20MC (Applied Biosystems) nickel-charged column, washed in wash buffer (10 mM PO_4^{2-}, pH 7.3, 250 mM KCl), and eluted on a linear gradient to 500 mM imidazole in the same buffer on an ÄKTA-FPLC system (GE Healthcare). Imidazole was removed by dialysis (SPECTRUMLABS.COM). Fusion proteins were then applied to a 60 ml Amylose (New England Biolabs) column, washed in wash buffer, and eluted in maltose buffer (10 mM PO_4^{2-}, pH 7.3, 250 mM KCl, 10 mM maltose). The buffer was exchanged to (10 mM HEPES, pH 7.4, 50 mM KCl, 1 mM EDTA) by dialysis. The HMT-fusion protein was cleaved with TEV protease[84] (~300 μM TEV protease for 10 hr at 18 °C in the TEV buffer). Cleaved material was applied to a Poros20MC nickel column and coiled-coil peptides were collected in the flow-through. Needle-shaped crystals formed in the fraction tubes in this purification step. The flow-through was further concentrated in an Amicon centrifugal filter (Millipore) during which time more microcrystals formed. The needle-shaped crystals were collected and dissolved in one of three buffers, Mg^{2+} buffer (10 mM Tris, pH 8.0, 100 mM $MgCl_2$), guanidine buffer (50 mM Tris, pH 8.4, 300 mM guanidine, 3 mM EDTA), or acidic buffer (20 mM Na acetate, pH 5.0). Protein concentration was determined by absorbance (BCA Protein Assay Kit, PIERCE). For purification of SeMet TRPM7cc, 5 mM of 2-Mercaptoethanol was included in the purification buffer for each step. SeMet protein also formed microcrystals during purification. For SeMet TRPM7cc crystallization, 5 mM DTT was included in both the protein solution and reservoir solution.

Crystallization and Data Collection

TRPM7cc crystals were obtained by hanging-drop vapor-diffusion at 20°C. C121 crystals grew from mixtures of 1 μl peptide (5 mg ml^{-1} dissolved in the Mg^{2+} buffer) and 1 μl reservoir solution containing 100 mM Tris pH 8.0, 100 mM $MgCl_2$, 5–10% (v/v) isopropanol. C222 crystals from grew from mixtures of 1 μl peptide (5 mg ml^{-1} dissolved in the acidic buffer) and 1 μl reservoir solution containing 100 mM sodium acetate, pH 4.9, 70–140 mM $AmSO_4$ and 40–50% (v/v) Glycerol. Crystals appeared within ~1 day and reached full size in 3–4 days. TRPM7cc SeMet crystals were grown in the C222 crystallization conditions. For data collection, the C121 crystals were transferred to Paratone-N and flash-cooled in liquid nitrogen. C222 crystals were frozen directly from the drop in liquid nitrogen. Data were collected at ≤100 K at Advanced Lightsource Beamline 8.3.1 (Lawrence Berkeley National Laboratory, Berkeley, CA) equipped with a Quantum 210 CCD detector (Area Detector Systems) and at the SSRL Beamline 9-2 (Stanford Synchrotron Radiation Laboratory) equipped with a MarUSA MarMosaic -325 CCD detector and were processed with HKL2000 (HKL Research)[85].

Structure Determination

Three-wavelength MAD experiments were performed on the SeMet C222 crystals. Fourteen selenium positions were located using SOLVE[86]. After density modification the figure of merit

was 0.68. The initial model was built with RESOLVE[87] and ARP/warp[57]. The structure from the C121 crystal was solved by molecular replacement using the structure template from the C222 crystal by PHASER[58]. Model building, including automatic and manual addition of solvent molecules, was done in COOT[88]. The C121 crystal structure was refined to 2.01 Å using REFMAC5[89] with the inclusion of TLS parameters throughout refinement. Final TRPM7cc models contain two tetramers in the asymmetric unit of the C121 crystal.

Structure analysis

Models were evaluated using the PDB evaluation server. No residues were in Ramachandran plot disallowed regions. Buried surface areas were calculated from the difference of the accessible side chain surface areas of the tetramer structure and of the individual helical monomers using ArealMol of the CCP4 Suite [90]. Residues 1231– 1277 of TRPM7, Residues 4–31 of GCN4-E20C (PDB code: 2CCN), residues 7–27 of chain A and residues 34–52 of chain B of ROP (PDB code: 1ROP), residues 31–50 of WSPLP (PDB code: 1YOD), residues 340–355 of Lac Repressor (PDB code: 1LBI), residues 5–29 of GCN4-pAeLV (PDB code: 2R2V), residues 5–29 of SARS-C44 (PDB code: 1ZV7) and residues 6–27 of GCN4-PV (PDB code: 2B22) were used in the calculations. Three or four residues at the most N-terminal and at most C-terminal of the coiled-coil structures were omitted to minimize end effects. Coiled-coil parameters were calculated with TWISTER[91].

CD Spectroscopy

50 μM purified TRPM7cc in a buffer of 250 mM NaCl, 100 mM $MgCl_2$ and 10 mM Tris, pH 8.9 was analyzed with an Aviv Model 215 spectropolarimeter (Aviv Biomedical) equipped with a peltier device. Wavelength scans from 315 nm to 190 nm were taken at 4°C in a 2 mm pathlength cuvette. Thermal stability was assessed by monitoring $[\theta]_{222}$ every 2°C from 4 to 98°C with 1 min equilibration time at each step. Molar ellipticity per residue of the buffer-subtracted CD spectrum was calculated as a function of concentration, path length, and number of residues per monomer:

$$[\theta]_{MRD}=\theta/(c \bullet 1 \bullet NR)$$

where $[\theta]_{MRD}$ is the molar ellipticity per residue in deg•cm2 (dmol•res)−1, θ is the experimental ellipticity in millidegrees, M is the molecular mass of the peptide, c is the protein concentration in μM, l is the cuvette path length in cm, and NR is the number of residues in the peptide. The percent helicity was estimated by:

$$\%\text{helicity}=[\theta]_{222}/[\theta]^{\infty}_{222}(1 - i\kappa/N) \times 100$$

where $[\theta]_{222}$ is the experimental molar ellipticity per residue at 222 nm, $[\theta]^{\infty}_{222}$ is the molar ellipticity for a helix of infinite length at 222 nm (i.e., –39,500 deg•cm^2 $dmol^{-1}$), *i* is the number of helices, κ is a wavelength-specific constant with a value of 2.57 at 222 nm, and N is the number of peptide residues[65].

Size Exclusion Chromatography

100 μl TRPM7cc peptide (500 μM peptide in 300 mM KCl, 100 mM $MgCl_2$, 50 mM Tris, pH 8.0) was passed through a Superdex75 HR 10/30 column (GE Healthcare) in the buffer (300 mM KCl, 100 mM $MgCl_2$, 50 mM Tris, pH 8.0) on an ÄKTA-FPLC system (GE Healthcare) at 4°C. Eluates were monitored at 280 nm over a flow rate of 0.4 ml min^{-1}. Elution volumes from at least three runs were averaged.

Equilibrium Sedimentation

Sedimentation equilibrium experiments were performed at 4°C in a Beckman Optima XL-A analytical ultracentrifuge (Beckman Coulter). TRM7cc peptide was dissolved in 150 μM in 400 mM KCl, 200 mM $MgCl_2$, 80 mM Tris, pH 8.0 and was loaded into a six-chamber analytical ultracentrifuge cuvette, using the dialyzate in the adjacent chamber as a blank. The molecular mass was calculated from a single-species exponential fit (Excel) to the distribution of concentration over the radius of the chamber as follows:

$$M=(2\mathrm{RT}/[(1-\bar{v}\rho)\bullet\omega^2])\bullet(d[\ln(c)]/d(r^2)$$

where M is the molecular weight in g mol^{-1}, R is the gas constant (8.314 J mol^{-1} K^{-1}), T is temperature in K, $\bar{v}$ is the partial specific volume of the protein in ml g^{-1}, ω is the angular velocity in rad s^{-1}, and r is the distance in cm from the center of the rotor to a given position in the cell [66]. Partial specific volume was calculated from the sum of the partial specific volumes of the individual residues in the protein. Solvent density was calculated from the components in the buffer. Residuals were calculated as the difference between the measured absorbance value and the predicted value extrapolated from the calculated molecular mass.

Disulfide exchange assay

Variants of the TRPM7 sequence with N-terminal Gly-Ser-Gly-Ser-Cys-Gly-Gly-Ser (N-TRPM7cc) or C-terminal Gly-Gly-Ser-Cys-Ser (C-TRPM7cc) were cloned into the pSV272-HMT vector. The Gly-Ser-Gly residues N-terminal to the cysteine in N-TRPM7cc were included to facilitate HPLC separation and unambiguous mass spec identification the heterodimer. N-TRPM7cc and C-TRPM7cc were expressed and purified separately. Purified peptides were mixed (1 mg ml^{-1} each) and incubated in a reducing buffer (300 mM Guanidine, 50 mM Tris-HCl pH8.4, 3 mM EDTA, 1mM DTT) for 0hr, 2hr and 48hr. After incubation the buffer was exchanged to 300 mM Guanidine, 50 mM Tris-HCl pH8.4, 3 mM EDTA using an Amicon centrifugal filter (Millipore) with several times of dilution to and increased to a final volume of 30mL. Disulfide bonds were generated by oxidation with 20 μM H_2O_2. Samples were concentrated into 100 μL and analyzed by HPLC using a linear water/acetonitrile gradient in 0.1% tri-fluoroacetic acid and a C-18 218TP54 analytical column (Vydac) monitored at λ=230 nm. Identities of disulfide-bonded species were confirmed by Mass Spectrometry in house or in the Vincent Coates Foundation Mass Spectrometry Laboratory (Stanford).

Supplementary Material

Refer to Web version on PubMed Central for supplementary material.

Acknowledgements

We thank P.R. Tsuruda for the HMT tagged TRPM7 clones, F. Van Petegem for help with data collection and processing, F. Findeisen for help with structure determination and refinement, M. Pioletti for comments on the manuscript, and Minor laboratory members for support at all stages of this work. This work was supported by grants to DLM from NIH/NIDCD and American Heart Association (AHA) and to YF from the Uehara Memorial Foundation, the AHA, and Japan Society for the Promotion of Science. DLM is an AHA Established Investigator.

REFERENCES

1. Venkatachalam K, Montell C. TRP channels. Annu Rev Biochem 2007;76:387–417. [PubMed: 17579562]
2. Clapham DE. TRP channels as cellular sensors. Nature 2003;426:517–524. [PubMed: 14654832]

3. Julius D, Basbaum AI. Molecular mechanisms of nociception. Nature 2001;413:203–210. [PubMed: 11557989]
4. Hille, B. Ion Channels of Excitable Membranes. 3rd edit. Sunderland, MA: Sinauer Associates, Inc.; 2001.
5. Yu FH, Catterall WA. The VGL-chanome: a protein superfamily specialized for electrical signaling and ionic homeostasis. Sci STKE 2004 2004:re15.
6. Kedei N, Szabo T, Lile JD, Treanor JJ, Olah Z, Iadarola MJ, Blumberg PM. Analysis of the native quaternary structure of vanilloid receptor 1. J Biol Chem 2001;276:28613–28619. [PubMed: 11358970]
7. Hoenderop JG, Voets T, Hoefs S, Weidema F, Prenen J, Nilius B, Bindels RJ. Homo- and heterotetrameric architecture of the epithelial Ca2+ channels TRPV5 and TRPV6. Embo J 2003;22:776–785. [PubMed: 12574114]
8. Tsuruda PR, Julius D, Minor DL Jr. Coiled coils direct assembly of a cold-activated TRP channel. Neuron 2006;51:201–212. [PubMed: 16846855]
9. Moiseenkova-Bell VY, Stanciu LA, Serysheva II, Tobe BJ, Wensel TG. Structure of TRPV1 channel revealed by electron cryomicroscopy. Proc Natl Acad Sci U S A 2008;105:7451–7455. [PubMed: 18490661]
10. Fleig A, Penner R. The TRPM ion channel subfamily: molecular, biophysical and functional features. Trends Pharmacol Sci 2004;25:633–639. [PubMed: 15530641]
11. Harteneck C. Function and pharmacology of TRPM cation channels. Naunyn Schmiedebergs Arch Pharmacol 2005;371:307–314. [PubMed: 15843919]
12. McKemy DD, Neuhausser WM, Julius D. Identification of a cold receptor reveals a general role for TRP channels in thermosensation. Nature 2002;416:52–58. [PubMed: 11882888]
13. Perez CA, Huang L, Rong M, Kozak JA, Preuss AK, Zhang H, Max M, Margolskee RF. A transient receptor potential channel expressed in taste receptor cells. Nat Neurosci 2002;5:1169–1176. [PubMed: 12368808]
14. Zhang Y, Hoon MA, Chandrashekar J, Mueller KL, Cook B, Wu D, Zuker CS, Ryba NJ. Coding of sweet, bitter, and umami tastes: different receptor cells sharing similar signaling pathways. Cell 2003;112:293–301. [PubMed: 12581520]
15. Nadler MJ, Hermosura MC, Inabe K, Perraud AL, Zhu Q, Stokes AJ, Kurosaki T, Kinet JP, Penner R, Scharenberg AM, Fleig A. LTRPC7 is a Mg.ATP-regulated divalent cation channel required for cell viability. Nature 2001;411:590–595. [PubMed: 11385574]
16. Perraud AL, Fleig A, Dunn CA, Bagley LA, Launay P, Schmitz C, Stokes AJ, Zhu Q, Bessman MJ, Penner R, Kinet JP, Scharenberg AM. ADP-ribose gating of the calcium-permeable LTRPC2 channel revealed by Nudix motif homology. Nature 2001;411:595–599. [PubMed: 11385575]
17. Runnels LW, Yue L, Clapham DE. TRP-PLIK, a bifunctional protein with kinase and ion channel activities. Science 2001;291:1043–1047. [PubMed: 11161216]
18. Chubanov V, Waldegger S, Mederos y Schnitzler M, Vitzthum H, Sassen MC, Seyberth HW, Konrad M, Gudermann T. Disruption of TRPM6/TRPM7 complex formation by a mutation in the TRPM6 gene causes hypomagnesemia with secondary hypocalcemia. Proc Natl Acad Sci U S A 2004;101:2894–2899. [PubMed: 14976260]
19. Li M, Jiang J, Yue L. Functional characterization of homo- and heteromeric channel kinases TRPM6 and TRPM7. J Gen Physiol 2006;127:525–537. [PubMed: 16636202]
20. Schmitz C, Dorovkov MV, Zhao X, Davenport BJ, Ryazanov AG, Perraud AL. The channel kinases TRPM6 and TRPM7 are functionally nonredundant. J Biol Chem 2005;280:37763–37771. [PubMed: 16150690]
21. Hara Y, Wakamori M, Ishii M, Maeno E, Nishida M, Yoshida T, Yamada H, Shimizu S, Mori E, Kudoh J, Shimizu N, Kurose H, Okada Y, Imoto K, Mori Y. LTRPC2 Ca2+-permeable channel activated by changes in redox status confers susceptibility to cell death. Mol Cell 2002;9:163–173. [PubMed: 11804595]
22. Perraud AL, Takanishi CL, Shen B, Kang S, Smith MK, Schmitz C, Knowles HM, Ferraris D, Li W, Zhang J, Stoddard BL, Scharenberg AM. Accumulation of free ADP-ribose from mitochondria mediates oxidative stress-induced gating of TRPM2 cation channels. J Biol Chem 2005;280:6138–6148. [PubMed: 15561722]

23. Erler I, Al-Ansary DM, Wissenbach U, Wagner TF, Flockerzi V, Niemeyer BA. Trafficking and assembly of the cold-sensitive TRPM8 channel. J Biol Chem 2006;281:38396–38404. [PubMed: 17065148]
24. Mei ZZ, Xia R, Beech DJ, Jiang LH. Intracellular coiled-coil domain engaged in subunit interaction and assembly of melastatin-related transient receptor potential channel 2. J Biol Chem 2006;281:38748–38756. [PubMed: 17060318]
25. Lupas AN, Gruber M. The structure of alpha-helical coiled coils. Adv Protein Chem 2005;70:37–78. [PubMed: 15837513]
26. Woolfson DN. The design of coiled-coil structures and assemblies. Adv Protein Chem 2005;70:79–112. [PubMed: 15837514]
27. Grigoryan G, Keating AE. Structural specificity in coiled-coil interactions. Curr Opin Struct Biol. 2008
28. Oakley MG, Hollenbeck JJ. The design of antiparallel coiled coils. Curr Opin Struct Biol 2001;11:450–457. [PubMed: 11495738]
29. Howard RJ, Clark KA, Holton JM, Minor J, Daniel L. Structural Insight into KCNQ (Kv7) Channel Assembly and Channelopathy. Neuron 2007;53:663–675. [PubMed: 17329207]
30. Wiener R, Haitin Y, Shamgar L, Fernandez-Alonso MC, Martos A, Chomsky-Hecht O, Rivas G, Attali B, Hirsch JA. The KCNQ1 (Kv7.1) COOH terminus, a multitiered scaffold for subunit assembly and protein interaction. J Biol Chem 2008;283:5815–5830. [PubMed: 18165683]
31. Jenke M, Sanchez A, Monje F, Stuhmer W, Weseloh RM, Pardo LA. C-terminal domains implicated in the functional surface expression of potassium channels. Embo J 2003;22:395–403. [PubMed: 12554641]
32. Ludwig J, Owen D, Pongs O. Carboxy-terminal domain mediates assembly of the voltage-gated rat ether-à-go-go potassium channel. EMBO J 1997;16:6337–6345. [PubMed: 9400421]
33. Zhong H, Lai J, Yau KW. Selective heteromeric assembly of cyclic nucleotide-gated channels. Proc Natl Acad Sci U S A 2003;100:5509–5513. [PubMed: 12700356]
34. Zhong H, Molday LL, Molday RS, Yau KW. The heteromeric cyclic nucleotide-gated channel adopts a 3A:1B stoichiometry. Nature 2002;420:193–198. [PubMed: 12432397]
35. Qian F, Germino FJ, Cai Y, Zhang X, Somlo S, Germino GG. PKD1 interacts with PKD2 through a probable coiled-coil domain. Nat Genet 1997;16:179–183. [PubMed: 9171830]
36. Tsiokas L, Kim E, Arnould T, Sukhatme VP, Walz G. Homo- and heterodimeric interactions between the gene products of PKD1 and PKD2. Proc Natl Acad Sci U S A 1997;94:6965–6970. [PubMed: 9192675]
37. Lee SY, Letts JA, Mackinnon R. Dimeric subunit stoichiometry of the human voltage-dependent proton channel Hv1. Proc Natl Acad Sci U S A 2008;105:7692–7695. [PubMed: 18509058]
38. Kreusch A, Pfaffinger PJ, Stevens CF, Choe S. Crystal structure of the tetramerization domain of the *Shaker* potassium channel. Nature 1998;392:945–948. [PubMed: 9582078]
39. Minor DL Jr. Lin YF, Mobley BC, Avelar A, Jan YN, Jan LY, Berger JM. The polar T1 interface is linked to conformational changes that open the voltage-gated potassium channel. Cell 2000;102:657–670. [PubMed: 11007484]
40. Cushman SJ, Nanao MH, Jahng AW, DeRubies D, Choe S, Pfaffinger PJ. Voltage dependent activation of potassium channels is coupled to T1 domain structure. Nature Struct. Biol 2000;7:403–407. [PubMed: 10802739]
41. Bixby KA, Nanao MH, Shen NV, Kreusch A, Bellamy H, Pfaffinger PJ, Choe S. Zn2+-binding and molecular determinants of tetramerization in voltage-gated K+ channels. Nat Struct Biol 1999;6:38–43. [PubMed: 9886290]
42. Penner R, Fleig A. The Mg2+ and Mg(2+)-nucleotide-regulated channel-kinase TRPM7. Handb Exp Pharmacol 2007:313–328. [PubMed: 17217066]
43. Montell C, Birnbaumer L, Flockerzi V. The TRP channels, a remarkably functional family. Cell 2002;108:595–598. [PubMed: 11893331]
44. Schmitz C, Perraud AL, Johnson CO, Inabe K, Smith MK, Penner R, Kurosaki T, Fleig A, Scharenberg AM. Regulation of vertebrate cellular Mg2+ homeostasis by TRPM7. Cell 2003;114:191–200. [PubMed: 12887921]

45. He Y, Yao G, Savoia C, Touyz RM. Transient receptor potential melastatin 7 ion channels regulate magnesium homeostasis in vascular smooth muscle cells: role of angiotensin II. Circ Res 2005;96:207–215. [PubMed: 15591230]
46. Aarts M, Iihara K, Wei WL, Xiong ZG, Arundine M, Cerwinski W, MacDonald JF, Tymianski M. A key role for TRPM7 channels in anoxic neuronal death. Cell 2003;115:863–877. [PubMed: 14697204]
47. Kim BJ, Lim HH, Yang DK, Jun JY, Chang IY, Park CS, So I, Stanfield PR, Kim KW. Melastatin-type transient receptor potential channel 7 is required for intestinal pacemaking activity. Gastroenterology 2005;129:1504–1517. [PubMed: 16285951]
48. Elizondo MR, Arduini BL, Paulsen J, MacDonald EL, Sabel JL, Henion PD, Cornell RA, Parichy DM. Defective skeletogenesis with kidney stone formation in dwarf zebrafish mutant for trpm7. Curr Biol 2005;15:667–671. [PubMed: 15823540]
49. Krapivinsky G, Mochida S, Krapivinsky L, Cibulsky SM, Clapham DE. The TRPM7 ion channel functions in cholinergic synaptic vesicles and affects transmitter release. Neuron 2006;52:485–496. [PubMed: 17088214]
50. Landman N, Jeong SY, Shin SY, Voronov SV, Serban G, Kang MS, Park MK, Di Paolo G, Chung S, Kim TW. Presenilin mutations linked to familial Alzheimer's disease cause an imbalance in phosphatidylinositol 4,5-bisphosphate metabolism. Proc Natl Acad Sci U S A 2006;103:19524–19529. [PubMed: 17158800]
51. McNulty S, Fonfria E. The role of TRPM channels in cell death. Pflugers Arch 2005;451:235–242. [PubMed: 16025303]
52. Touyz RM. Transient receptor potential melastatin 6 and 7 channels, magnesium transport, and vascular biology: implications in hypertension. Am J Physiol Heart Circ Physiol 2008;294:H1103–H1118. [PubMed: 18192217]
53. Schlingmann KP, Weber S, Peters M, Niemann Nejsum L, Vitzthum H, Klingel K, Kratz M, Haddad E, Ristoff E, Dinour D, Syrrou M, Nielsen S, Sassen M, Waldegger S, Seyberth HW, Konrad M. Hypomagnesemia with secondary hypocalcemia is caused by mutations in TRPM6, a new member of the TRPM gene family. Nat Genet 2002;31:166–170. [PubMed: 12032568]
54. Walder RY, Landau D, Meyer P, Shalev H, Tsolia M, Borochowitz Z, Boettger MB, Beck GE, Englehardt RK, Carmi R, Sheffield VC. Mutation of TRPM6 causes familial hypomagnesemia with secondary hypocalcemia. Nat Genet 2002;31:171–174. [PubMed: 12032570]
55. Yamaguchi H, Matsushita M, Nairn AC, Kuriyan J. Crystal structure of the atypical protein kinase domain of a TRP channel with phosphotransferase activity. Mol Cell 2001;7:1047–1057. [PubMed: 11389851]
56. McDonnell AV, Jiang T, Keating AE, Berger B. Paircoil2: improved prediction of coiled coils from sequence. Bioinformatics 2006;22:356–358. [PubMed: 16317077]
57. Perrakis A, Morris R, Lamzin VS. Automated protein model building combined with iterative structure refinement. Nat Struct Biol 1999;6:458–463. [PubMed: 10331874]
58. Storoni LC, McCoy AJ, Read RJ. Likelihood-enhanced fast rotation functions. Acta Crystallogr D Biol Crystallogr 2004;60:432–438. [PubMed: 14993666]
59. Deng Y, Liu J, Zheng Q, Eliezer D, Kallenbach NR, Lu M. Antiparallel four-stranded coiled coil specified by a 3-3-1 hydrophobic heptad repeat. Structure 2006;14:247–255. [PubMed: 16472744]
60. Slovic AM, Stayrook SE, North B, Degrado WF. X-ray structure of a water-soluble analog of the membrane protein phospholamban: sequence determinants defining the topology of tetrameric and pentameric coiled coils. J Mol Biol 2005;348:777–787. [PubMed: 15826670]
61. Yadav MK, Leman LJ, Price DJ, Brooks CL 3rd, Stout CD, Ghadiri MR. Coiled coils at the edge of configurational heterogeneity. Structural analyses of parallel and antiparallel homotetrameric coiled coils reveal configurational sensitivity to a single solvent-exposed amino acid substitution. Biochemistry 2006;45:4463–4473. [PubMed: 16584182]
62. Banner DW, Kokkinidis M, Tsernoglou D. Structure of the ColE1 rop protein at 1.7 A resolution. J Mol Biol 1987;196:657–675. [PubMed: 3681971]
63. Crick FHC. The packing of α-helices: Simple coiled-coils. Acta. Cryst 1953;6:689–697.
64. Gottschalk KE. A coiled-coil structure of the alphaIIbbeta3 integrin transmembrane and cytoplasmic domains in its resting state. Structure 2005;13:703–712. [PubMed: 15893661]

65. Chen YH, Yang JT, Chau KH. Determination of the helix and beta form of proteins in aqueous solution by circular dichroism. Biochemistry 1974;13:3350–3359. [PubMed: 4366945]
66. Laue TM. Sedimentation equilibrium as a thermodynamic tool. Meth. Enzymol 1995;259:427–453. [PubMed: 8538465]
67. Monera OD, Zhou NE, Kay CM, Hodges RS. Comparison of antiparallel and parallel two-stranded alpha-helical coiled-coils. Design, synthesis, and characterization. J Biol Chem 1993;268:19218–19227. [PubMed: 8366074]
68. Monera OD, Zhou NE, Lavigne P, Kay CM, Hodges RS. Formation of parallel and antiparallel coiled-coils controlled by the relative positions of alanine residues in the hydrophobic core. J Biol Chem 1996;271:3995–4001. [PubMed: 8626731]
69. Schnarr NA, Kennan AJ. pH-Switchable strand orientation in peptide assemblies. Org Lett 2005;7:395–398. [PubMed: 15673248]
70. Harbury PB, Zhang T, Kim PS, Alber T. A switch between two-, three-, and four-stranded coiled coils in GCN4 leucine zipper mutants. Science 1993;262:1401–1407. [PubMed: 8248779]
71. Deutsch C. Potassium channel ontogeny. Annu Rev Physiol 2002;64:19–46. [PubMed: 11826262]
72. Deutsch C. The birth of a channel. Neuron 2003;40:265–276. [PubMed: 14556708]
73. Papazian DM. Potassium channels: some assembly required. Neuron 1999;23:7–10. [PubMed: 10402187]
74. Lewis M, Chang G, Horton NC, Kercher MA, Pace HC, Schumacher MA, Brennan RG, Lu P. Crystal structure of the lactose operon repressor and its complexes with DNA and inducer. Science 1996;271:1247–1254. [PubMed: 8638105]
75. Li M, Jan YN, Jan LY. Specification of subunit assembly by the hydrophilic amino-terminal domain of the Shaker potassium channel. Science 1992;257:1225–1230. [PubMed: 1519059]
76. Gulbis JM, Zhou M, Mann S, MacKinnon R. Structure of the cytoplasmic β subunit-T1 assembly of voltage-dependent K^+ channels. Science 2000;289:123–127. [PubMed: 10884227]
77. Long SB, Campbell EB, Mackinnon R. Crystal structure of a mammalian voltage-dependent Shaker family K+ channel. Science 2005;309:897–903. [PubMed: 16002581]
78. Pioletti M, Findeisen F, Hura GL, Minor DL Jr. Three-dimensional structure of the KChIP1-Kv4.3 T1 complex reveals a cross-shaped octamer. Nat Struct Mol Biol 2006;13:987–995. [PubMed: 17057713]
79. Kass RS, Kurokawa J, Marx SO, Marks AR. Leucine/isoleucine zipper coordination of ion channel macromolecular signaling complexes in the heart. Roles in inherited arrhythmias. Trends Cardiovasc Med 2003;13:52–56. [PubMed: 12586439]
80. Haitin Y, Attali B. The C-terminus of Kv7 channels: a multifunctional module. J Physiol 2008;586:1803–1810. [PubMed: 18218681]
81. Marx SO, Kurokawa J, Reiken S, Motoike H, D'Armiento J, Marks AR, Kass RS. Requirement for a macromolecular signaling complex for β adrenergic receptor modulation of the KCNQ1-KCNE1 potassium channel. Science 2002;295:496–499. [PubMed: 11799244]
82. Van Petegem F, Clark KA, Chatelain FC, Minor DL Jr. Structure of a complex between a voltage-gated calcium channel beta-subunit and an alpha-subunit domain. Nature 2004;429:671–675. [PubMed: 15141227]
83. Studier FW. Protein production by auto-induction in high density shaking cultures. Protein Expr Purif 2005;41:207–234. [PubMed: 15915565]
84. Kapust RB, Tozser J, Fox JD, Anderson DE, Cherry S, Copeland TD, Waugh DS. Tobacco etch virus protease: mechanism of autolysis and rational design of stable mutants with wild-type catalytic proficiency. Protein Eng 2001;14:993–1000. [PubMed: 11809930]
85. Otwinowski Z, Minor W. Processing of X-ray diffraction data collected in oscillation mode. Meth. Enzy 1997;276:307–326.
86. Terwilliger TC, Berendzen J. Automated MAD and MIR structure solution. Acta Crystallogr D Biol Crystallogr 1999;55:849–861. [PubMed: 10089316]
87. Terwilliger TC. SOLVE and RESOLVE: automated structure solution and density modification. Methods Enzymol 2003;374:22–37. [PubMed: 14696367]

88. Emsley P, Cowtan K. Coot: model-building tools for molecular graphics. Acta Crystallogr D Biol Crystallogr 2004;60:2126–2132. [PubMed: 15572765]

89. Murshudov GN, Vagin AA, Dodson EJ. Refinement of macromolecular structures by the maximum-likelihood method. Acta Crystallogr D Biol Crystallogr 1997;53:240–255. [PubMed: 15299926]

90. C. C. P.4. The CCP4 Suite: programs for protein crystallography. Acta Crystallogr A 1994;50:760–763.

91. Strelkov SV, Burkhard P. Analysis of alpha-helical coiled coils with the program TWISTER reveals a structural mechanism for stutter compensation. J Struct Biol 2002;137:54–64. [PubMed: 12064933]

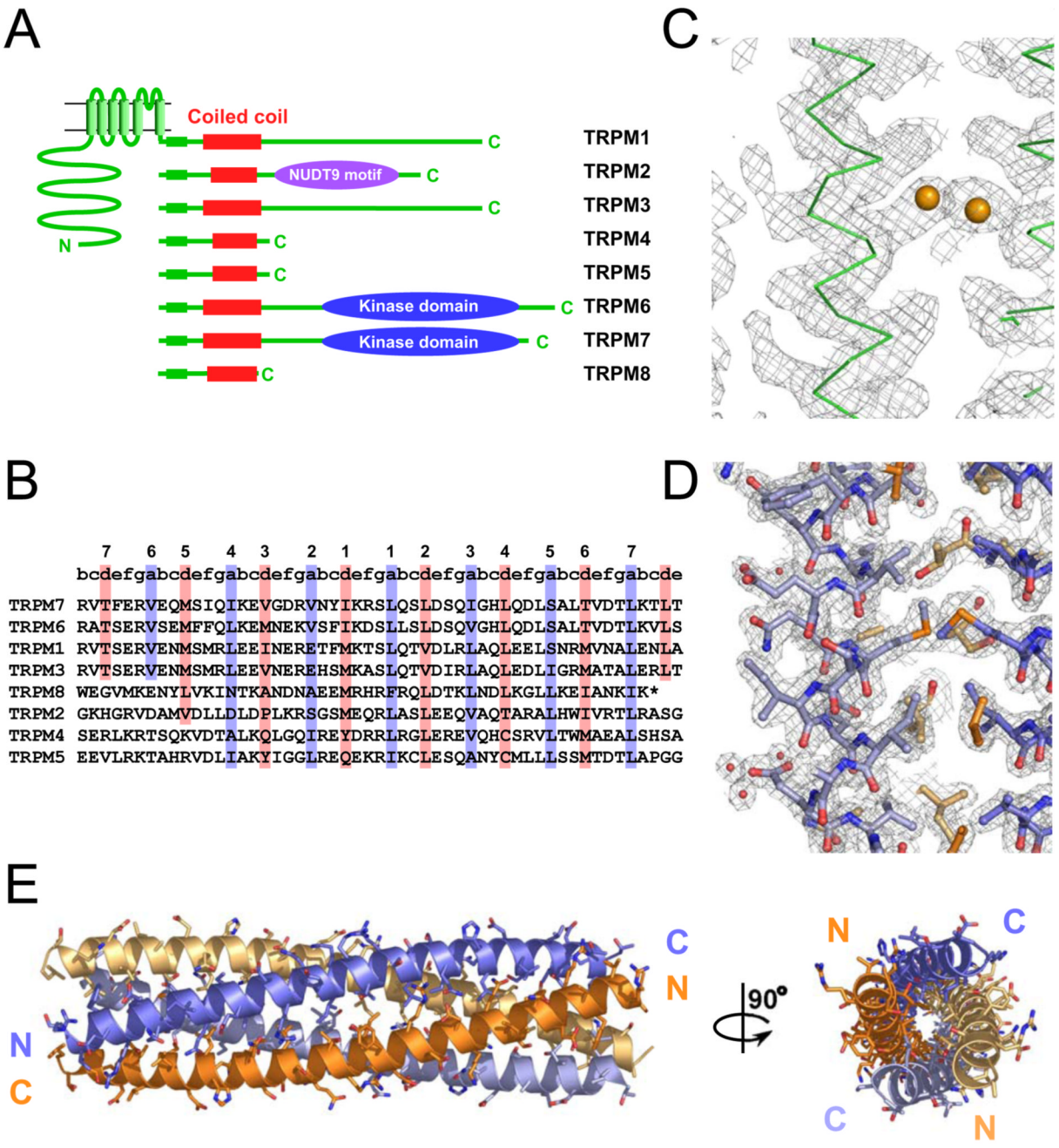

Figure 1. Structure of the TRPM channel coiled-coil assembly domain

A, Cartoon of TRPM family subunits. Conserved TRP domain (green box) and coiled-coil domain (red box) are indicated. Kinase domains of TRPM6 and TRPM7 and the TRPM2 NUTD9 motif are shown as ovals. **B,** Sequence alignment TRPM coiled-coil domains. Positions of the coiled-coil heptad repeat (abcdefg) are indicated below the alignment. Coiled-coil residues occupying the ‘a’ and ‘d’ positions are denoted by blue and red, respectively. Layer position for each residue in TRPM7cc is indicated above the alignment. Depicted sequences are as follows: rat TRPM7 1230–1282 (XM_001056331), rat TRPM6 1173–1225 (XP_219747), human TRPM1 1183–1235 (NP_002411), human TRPM3 1244–1296 (Q9HCF6), rat TRPM8 1055–1104 (NP_599198), rat TRPM2 1155–1207 (BAE72117),

mouse TRPM4 1144–1196 (AAH96475), and mouse TRPM5 1071–1126 (AAI33713). **C,** TRPM7cc MAD experimental density map contoured at 1.0 σ. α-helix backbone and heavy atoms positions are indicated as green line trace and orange spheres, respectively. **D,** Final refined structure (sticks) and 2Fo-Fc composite-omit map built by random omission of 5% of model. Maps are contoured at 1.0 σ. **E,** (Left) TRPM7cc ribbon diagram. Pairs of similarly oriented helices are shown as blue/light blue and orange/light orange. Side chains are shown in stick representation. N- and C-terminal ends of the subunits are indicated. (Right) Axial view of TRPM7cc.

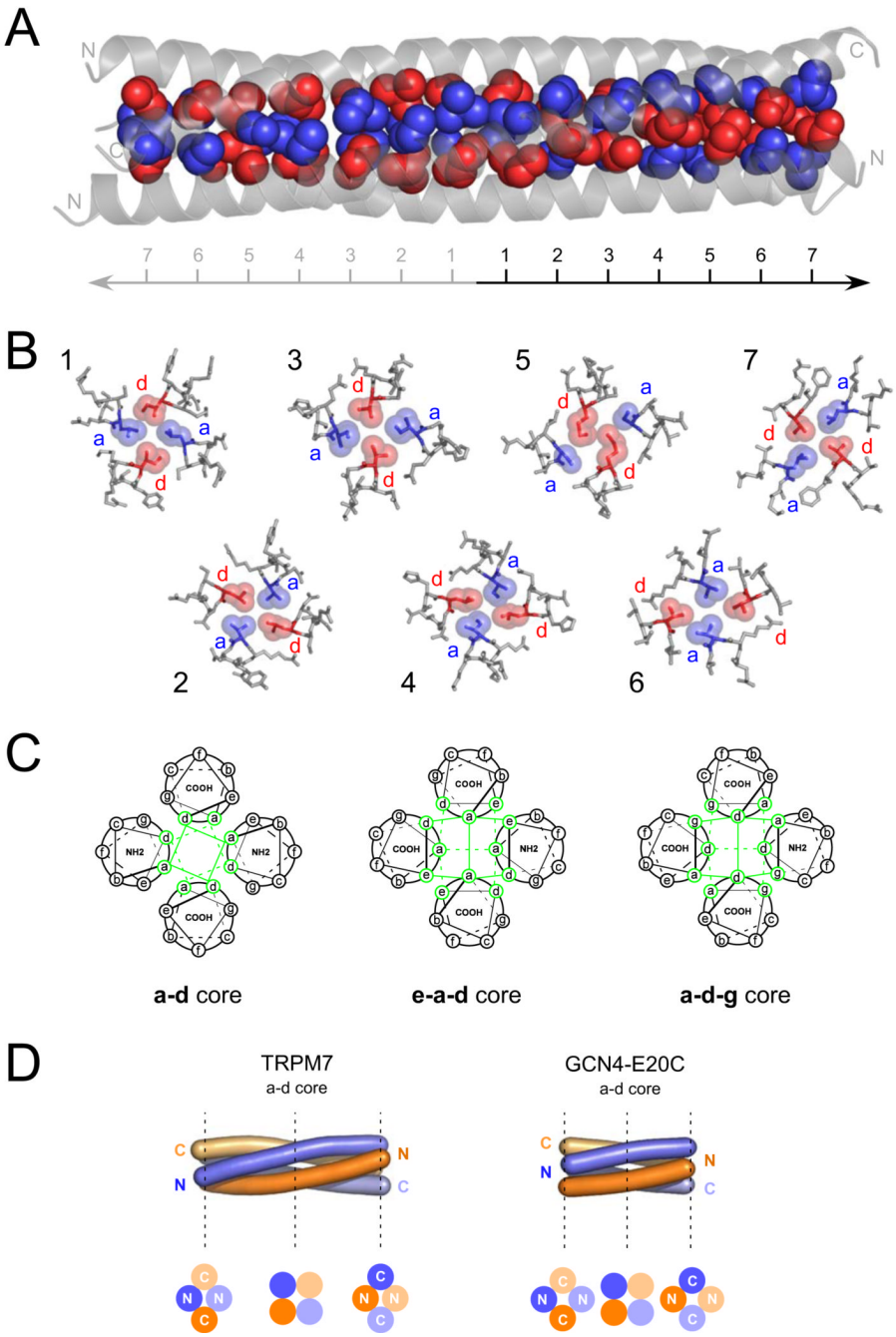

Figure 2. Core packing in the TRPM channel Coiled-Coil Domain

A, Coiled-coil core hydrophobic layers. van der Waals spheres depicting the sidechains of the 'a' (blue) and 'd' (red) layers on a ribbon backbone (gray) are shown. Layer numbers and N- and C-terminal ends of the coiled-coil are indicated. **B,** Geometry of individual coiled-coil layers. Ball-and-stick representations show each layer of the core. 'a' and 'd' positions are colored as in **A**. Layer numbers are indicated in black. **C,** Helical wheel representations for the different antiparallel homotetrameric coiled-coil core-packing arrangements. Heptad repeat positions are labeled a-g. Core-forming positions are highlighted in green and solid or dashed lines link positions lying in the same layer. **D,** Sausage diagram of TRPM7cc and GCN4-E20C

61 ‘a-d’ core antiparallel coiled-coils. Cross-sections of the helical arrangements are shown for the center and ends of the coils.

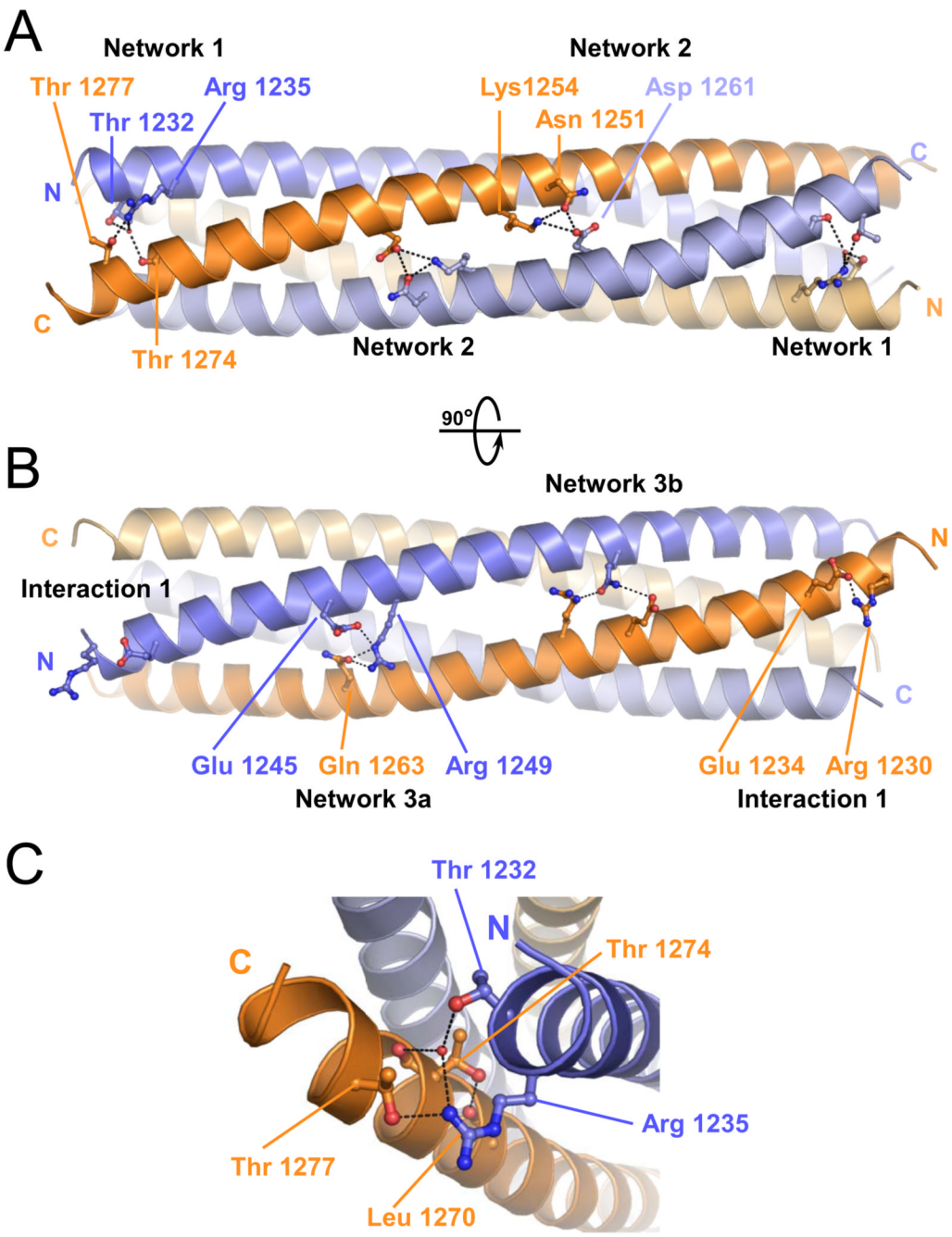

Figure 3. TRPM7cc electrostatic interactions

A, TRPM7cc Network1 and Network 2. **B,** TRPM7cc Network3a, Network 3b, and intrasubunit Interaction 1. **C,** Closeup view of Network 1 and the sidechain-backbone hydrogen bond of Layer 6 (Thr1274). In all panels sidechains are shown as ball-and stick, hydrogen bonds are indicated as dotted lines, and residue carbon atoms and labels are color coded to indicate the subunit of origin.

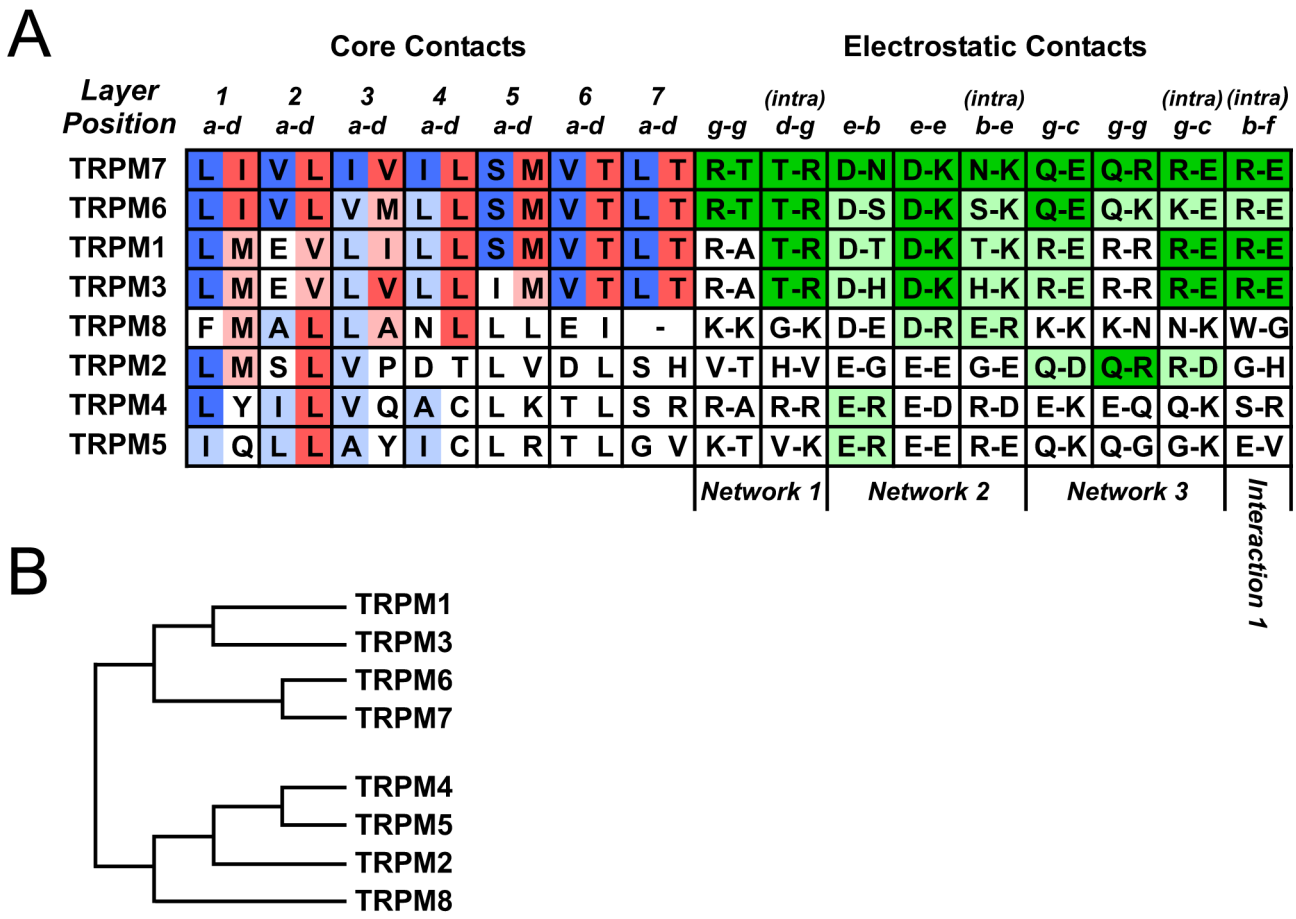

Figure 4. Structure-based comparison of TRPM coiled-coils

A, Comparative interaction mapping of TRPM subtypes. Column labels identify residue positions involved in the ‘a-d’ core layers and electrostatic networks. Filled boxes indicate conserved positions. Shaded boxes indicate nonconserved residues that remain capable of supporting interactions similar to those observed in TRPM7cc. White boxes indicate nonconserved positions. **B,** TRPM channel phylogentic comparison[1].

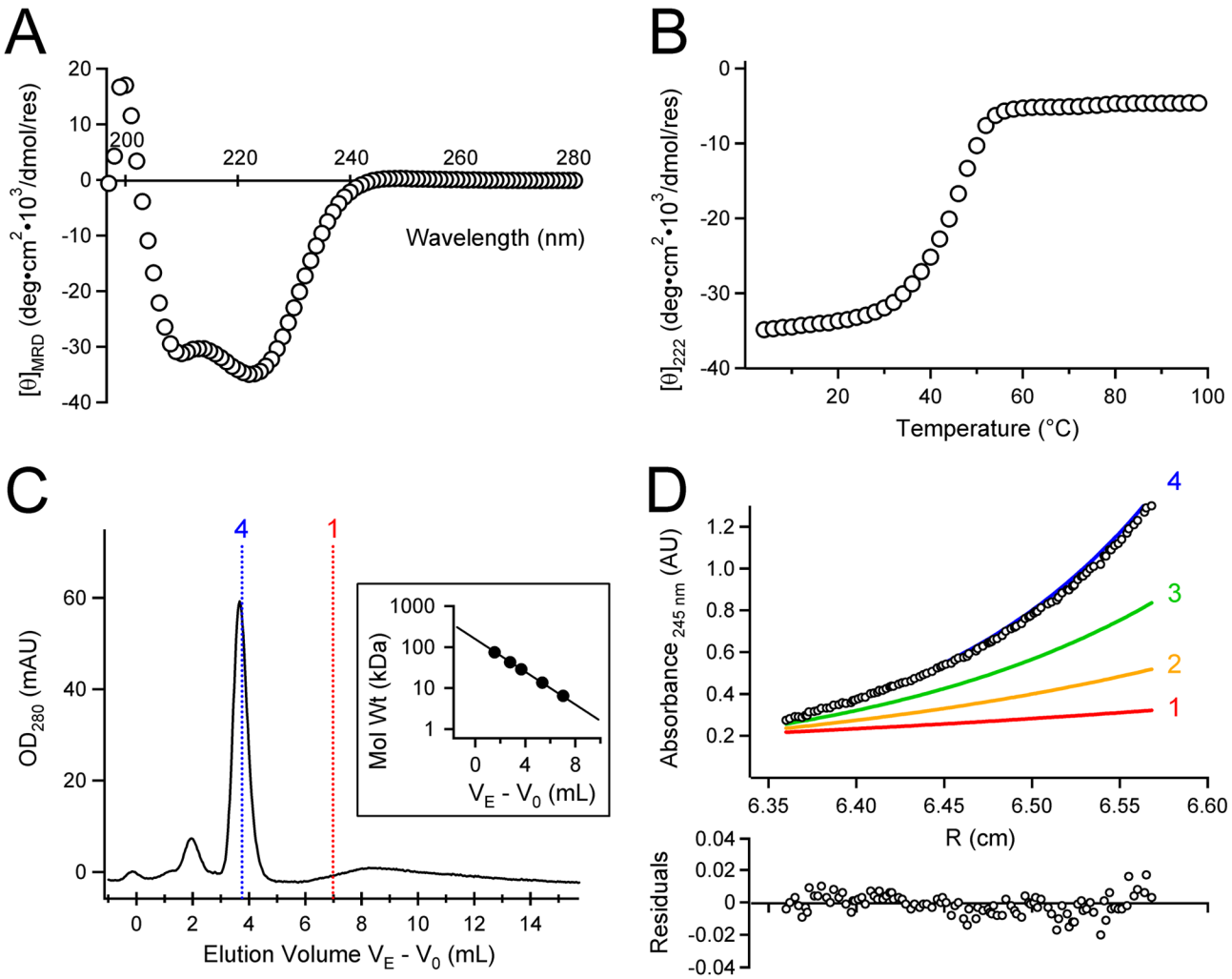

Figure 5. TRPM7cc solution properties

A, TRPM7cc Circular dichroism (CD) spectrum at 4°C. **B,** Temperature dependence of the TRPM7cc circular dichroism signal at 222 nm. **C,** TRPM7cc stoichiometry determined by Superdex 75 (Amersham Biosciences) size exclusion chromatography. Horizontal axis shows elution volume, V_E, relative to the void elution volume of blue dextran (V_0) (ml). Dotted lines indicate predicted elution volume of tetrameric and monomeric peptides. (Inset) standard curve used to calculate molecular weight of eluted peptides. TRPM7cc molecular weights are 26.7 kD, observed; 6.4 kD, expected monomer; 25.6 kD, expected tetramer. **D,** Sedimentation equilibrium of TRPM7cc. Equilibrium distribution of TRPM7cc (open circles) measured by absorbance at 245 nm as a function of radial distance at 20,000 rpm and 4°C. Raw data are shown relative to predicted distribution curves for monomeric (red), dimeric (yellow), trimeric (green), and tetrameric (blue), species. Residuals for the tetrameric distribution are shown.

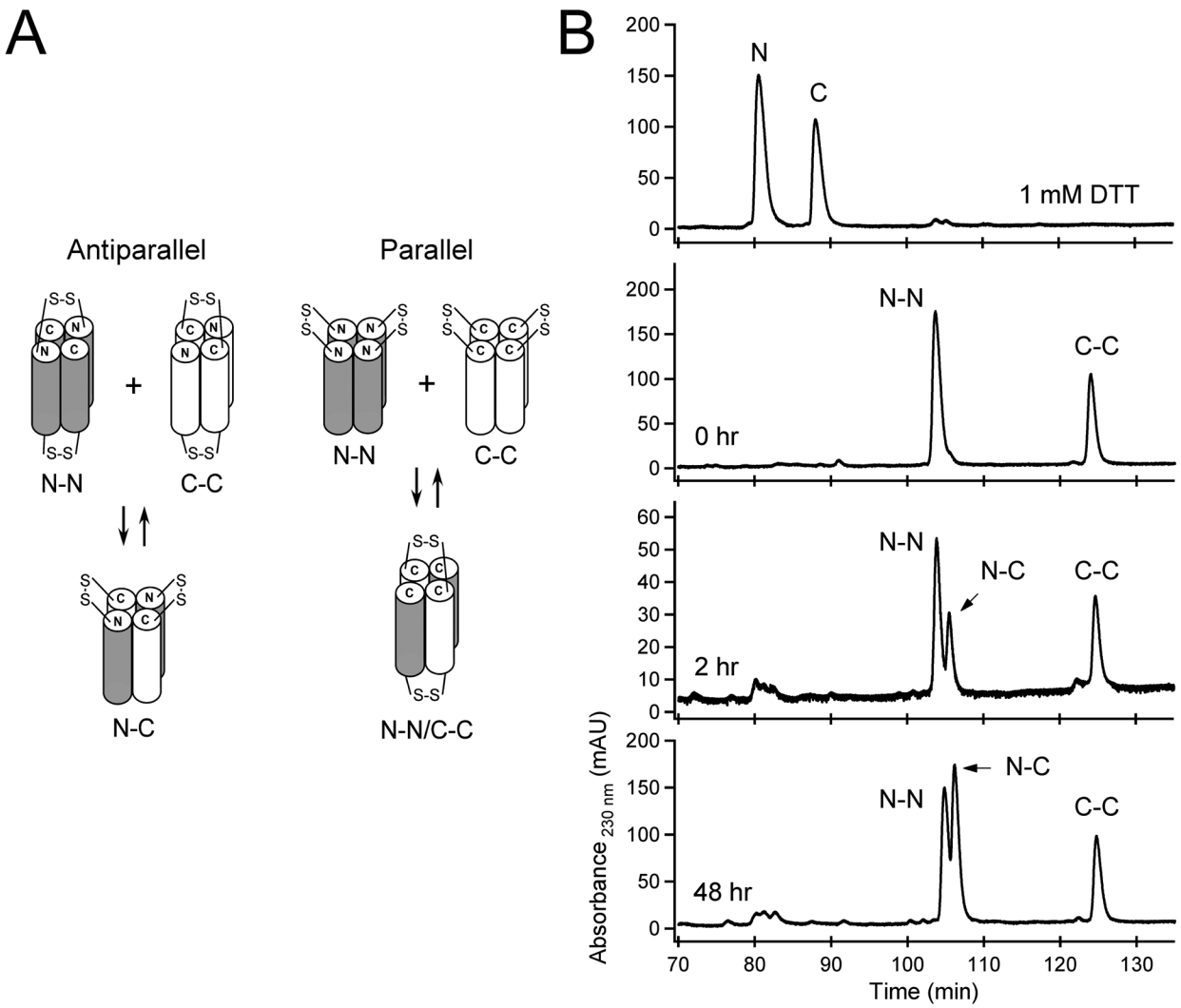

Figure 6. TRPM7cc helices are arranged antiparallel in solution

A, Schematic diagrams of expected disulfide bond species starting with the tetramers shown on the top and following subunit exchange to form the heteromeric species on the bottom for antiparallel (left) and parallel (right) orientations. Parallel tetramers will form only homodimeric disulfide-bonded species (right), whereas antiparallel tetramers will form homomeric and antiparallel heterodimeric disulfide bonded pairs (left). **B,** TRPM7cc disulfide exchange assay shows presence of antiparallel helices. Top, reduced starting mixture of N-TRPM7cc and C-TRPM7cc tetramers show single peaks for the monomeric, reduced peptides. Second from top, oxidation of reduced tetramers immediately after mixing (0 hr) shows two homomeric species, N-N and C-C. Bottom two traces, disulfide-bonded antiparallel heterodimer, N-C, appears after subunit exchange (2 hr, and 48 hr).

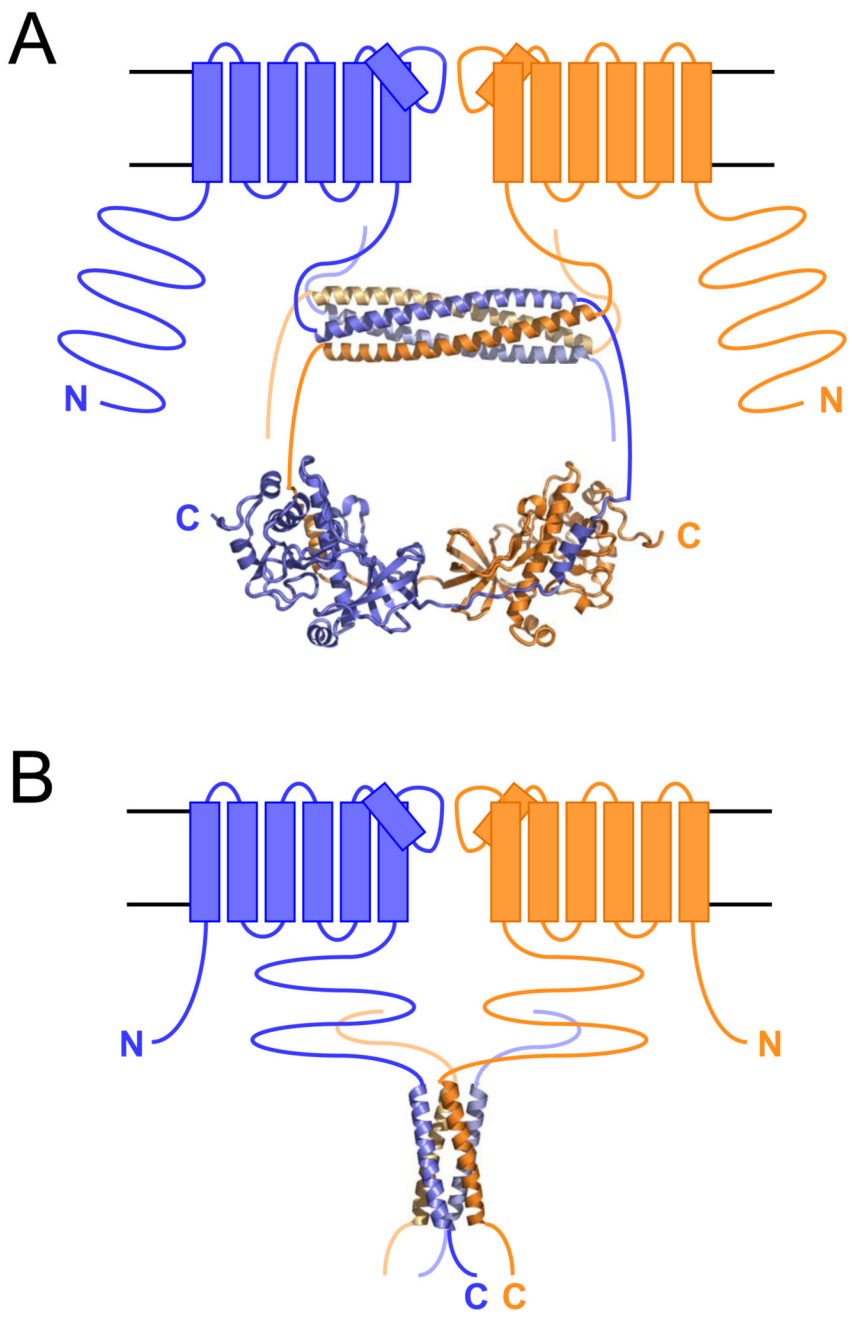

Figure 7. Comparisons between TRPM7 and Kv7 channel assembly domains

A, Cartoon model of TRPM7 showing the relationship between the antiparallel assembly domain, transmembrane domains, and dimeric kinase domains. For display purposes, the kinase domain dimer is shown linked to the C-terminal ends of antiparallel assembly domain strands. The other arrangement, kinase dimers linked to parallel strands is also possible. Presently available data do not favor one arrangement over the other. **B,** Cartoon model of a Kv7 channel. The parallel coiled-coil assembly domain, 1OVC [29], is shown as ribbons. In both panels only two of the four transmembrane domains are shown.

Table I

Data collection and refinement statistics

Data collection	**TRPM7cc native**		**TRPM7cc SeMet**		
			Peak	**Inflection**	**Remote**
Resolution (A)	50.0-2.00 (2.07-2.00)	50.0-2.40 (2.44-2.40)	50.0-2.70 (2.75-2.70)	50.0-2.80 (2.85-2.80)	50.0-2.80 (2.85-2.80)
Space group	C121	C222	C222	C222	C222
Cell dimensions: a, b, c (Å)	146.26, 35.67, 100.32	93.21, 185.45, 72.65	92.69, 185.40, 72.65	93.14, 185.95, 72.86	93.77, 186.57, 73.10
Cell dimensions: α,β,γ(°)	90.00, 124.46, 90.00	90.00, 90.00, 90.00	90.00, 90.00, 90.00	90.00, 90.00, 90.00	90.00, 90.00, 90.00
R_{sym}	12.1 (35.9)	7.8 (52.3)	9.0 (47.3)	9.4 (49.2)	8.7 (41.8)
Wavelength	0.9796	1.11588	0.97926	0.97976	1.01952
$I/\sigma I$	11.0 (2.3)	18.3 (2.3)	17.7 (2.8)	18.1 (2.6)	20.1 (3.1)
Completeness (%)	97.7 (85.4)	99.9 (99.8)	99.9 (98.9)	99.8 (97.6)	99.9 (98.1)
Redundancy	3.3 (2.8)	4.2 (4.1)	7.7 (6.7)	7.7 (6.3)	7.7 (6.4)
Refinement					
Resolution (Å)	2.01	2.40			
No. reflections	26765	23978			
R_{work}/R_{free}	18.8 / 24.8	22.7 / 29.4			
Total protein atoms	3372				
Total water atoms	297				
Average B-factors: protein (Å)	26.9				
Average B-factors: water (Å)	34.1				
RMSD in bond lengths (Å)	0.021				
RMSD in bond angles (°)	1.783				

Values in parentheses are for the highest-resolution shell

$$R_{sym} = \sum_{hkl} \sum_{i} [\, |I_\tau(hkl) - \langle I(hkl) \rangle| \Big/ I_i(hkl) \,]$$

$$R_{work} = \sum_{hkl} \big| \, |F_{obs}(hkl)| - |F_{calc}(hkl)| \, \big| \Big/ \sum_{hkl} |F_{obs}(hkl)|$$

R_{free} = R_{work} calculated using 5% of the reflection data chosen randomly and omitted from the start of refinement.

Table II

Comparison of coiled-coil parameters

Buried Surface area (%)								
			a-d core			**e-a-d** core		**a-d-g** core
Position	TRPM7cc	GCN4 E20C	WSPLP	Rop	Lac repressor	GCN4 pAeLV	SARS-C44	GCN4-pV
a	98	99	100	99	100	100	90	89
b	15	22	8	25	41	39	0	0
c	16	5	4	19	0	1	37	35
d	98	95	96	98	86	94	99	94
e	62	76	74	79	98	93	27	28
f	0	0	0	0	10	3	5	1
g	61	45	54	66	28	50	94	90
Knob-against-knob pattern								
			a-d core			**e-a-d** core		**a-d-g** core
Position	TRPM7cc a-a/d-d	GCN4 E20C a-a	WSPLP a-a	Rop d-d	Lac repressor a-a	GCN4 pAeLV a-a	SARS-C44 d-d	GCN4-pV d-d
Coiled-coil parameters								
Superhelical parameter	TRPM7	GCN4 E20C	WSPLP	Rop	Lac repressor	GCN4 pAeLV	SARS C44	GCN4-pV
Supercoil radius (Å)	7.3	7.6	8.0	7.4	6.8	7.2	7.2	7.4
Residues per superhelix turn	113	129	171	128	143	125	136	107
Supercoil pitch (Å)	165	189	252	187	213	182	199	156
α-Helical parameters								
α-Helix radius (A)	2.29	2.29	2.28	2.30	2.28	2.29	2.29	2.25
Residues per turn	3.61	3.59	3.60	3.61	3.59	3.60	3.60	3.58
Rise per residue (A)	1.52	1.51	1.51	1.51	1.52	1.51	1.50	1.53

Table III

TRPM7cc equilibrium sedimentation data

Concentration	Observed molecular weight (kDa)	Oligomeric state	n
250 μM	26.2 ± 2.6	4.1 ± 0.4	3
150 μM	25.4 ± 0.7	4.0 ± 0.1	3
70 μM	23.7 ± 0.7	3.7 ± 0.1	3
30 μM	25.4 ± 1.0	4.0 ± 0.1	4
Average	25.2 ± 1.5	4.0 ± 0.2	13

Monomer molecular weight is 6.3 kDa. Errors indicate standard deviation.